Selection in a 3D microtomographic image the region with the highest quality

A S Kornilov[1,2], I V Safonov[1], A V Goncharova[2] and I V Yakimchuk[1]

[1]Schlumberger Moscow Research, Pudovkina 13, Moscow, Russia, 119285
[2]National Research Nuclear University MEPhI, Kashirskoe shosse 31, Moscow, Russia, 115409

e-mail: kranton94@mail.ru

Abstract. We present an algorithm for processing of X-ray microtomographic (micro-CT) images that allows automatic selection of a sub-volume having the best visual quality for further mathematical simulation, for example, flow simulation. Frequently, an investigated sample occupies only a part of a volumetric image or the sample can be into a holder; a part of the image can be cropped. For each 2D slice across the Z-axis of an image, the proposed method locates a region corresponding to the sample. We explored applications of several existing blind quality measures for an estimation of the visual quality of a micro-CT image slice. Some of these metrics can be applied to ranking the image regions according to their quality. Our method searches for a cubic area located inside regions belonging to the sample and providing the maximal sum of the quality measures of slices crossing the cube across the Z-axis. The proposed technique was tested on synthetic and real micro-CT images of rocks.

1. Introduction

In the last decade, X-ray microtomography (micro-CT) has been actively used for analyzing of rock, soil, granular materials [1] and building their 3D models for a Digital Rock [2]. One of the applications of these digital models is a flow modelling of a multiphase fluid [3]. A typical micro-CT image can have size up to ~4000^3 voxels. Some systems allow getting even larger images. However, the sample under study occupies only part of the image or can be in the holder. For mathematical modelling, researchers often use only a sample fragment of a cubic form with sides from 400 to 1000 voxels. Thus, there is a task of cropping a fragment from a whole micro-CT image, which is suitable and, in some sense, optimal for further analysis. Currently, an operator performs this procedure manually. The quality of the micro-CT image varies in the image volume, individual parts of the sample, for example, dense inclusions, can significantly affect the quality [4]. For a reasonable fragment selection, the operator needs to view several hundred slices of a 3D image. The selection process takes considerable time and depends on the subjective opinion of the operator. So, the development of an automatic quick and formalized algorithm of the fragment selection for mathematical modelling is an important problem.

The complexity of this problem is explained by the huge variety of images that can be on the input of the algorithm. This diversity is caused not only by the variety of scanned samples but also by

features of various microtomographic systems and parameters of image reconstruction algorithms. In addition, certain tomography artifacts can be differently suppressed by various reconstruction software. Frequently, only a part of an original reconstructed tomographic image relates to a sample. And also the software of a micro-CT system reconstructs from shadow projections an image having a bit depth of 8 or 16 bits per voxel.

Figure 1 demonstrates several examples of 2D slices perpendicular to the Z axis. These images were obtained using different micro-CT systems. A granular material is placed in a cylindrical holder, which is completely inside the field of view, non-reconstructed areas in the corners of the image are filled by gray (figure 1a). A cylindrical sample of sandstone is completely in the field of view, the areas in the corners are filled by gray (figure 1b). A cylindrical sandstone sample is completely in the field of view but is off-center; unreconstructed areas are filled by black (figure 1c). Note, the holder is not of interest for further analysis. In the following example, scanning is performed inside a sample, unreconstructed corner areas are darker and blurred (figure 1d) than a center zone. A piece of an arbitrary shape sample is completely in the field of view (figure 1e). A rectangular fragment is cropped from an original reconstructed image (figure 1f). In addition, several dozen slices at the top and bottom of a 3D image may not contain the sample. They can contain a holder or air.

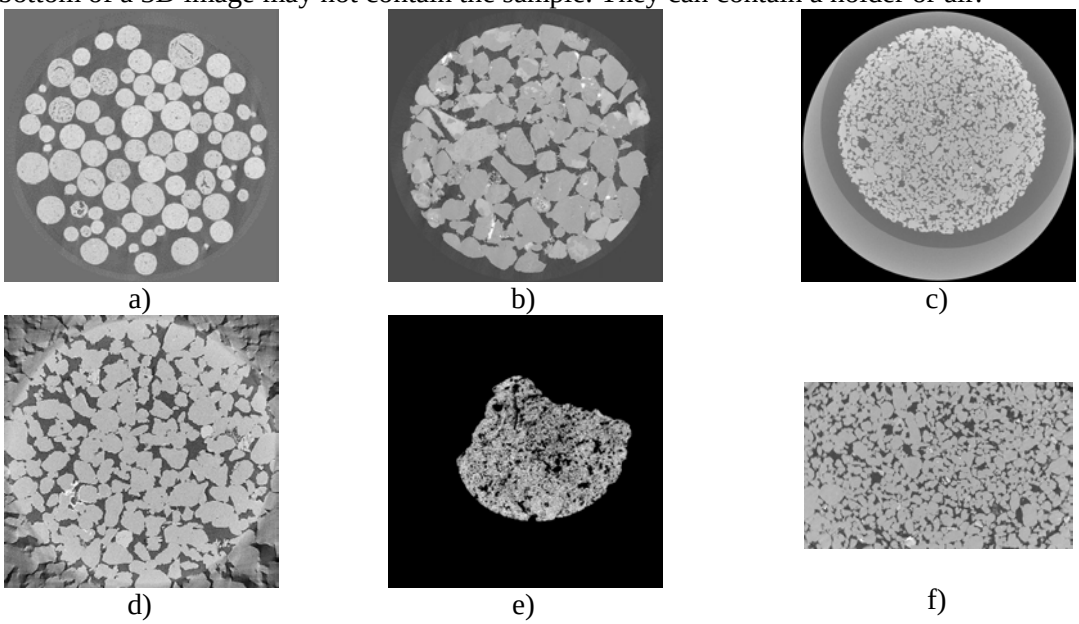

Figure 1. Examples of slices of various micro-CT images.

One more challenge is a formalization of a criterion for a selection of a fragment for further modelling. Which one of the many possible fragments to choose? It is reasonable to crop the fragment optimal from the point of view of some criterion. What can the criterion be in this case? Ideally, the criterion should depend on the objectives of the subsequent modeling. For example, to simulate the fluid flow, the criterion may be based on porosity or coherence of the pore structure. However, regardless of the methods and objectives of the subsequent analysis, we can say that we are interested to determine the most qualitative fragment in terms of visual assessment.

An important requirement for the developed algorithm and software is a high speed of the micro-CT image analysis. The processing time should be substantially less than the time required for the selection of the suitable fragment manually. We propose a fast algorithm that automatically selects from a micro-CT image a fragment of a given size that has the highest visual quality assessment.

2. Algorithm for selection of micro-CT image region

2.1. Main ideas

We propose to select a convex region related to the sample on each slice of the 3D image and evaluate the image quality in this area. Then we determine whether it is possible to inscribe a cube of a given

size into selected regions of consecutive slices and calculate the image quality estimation for the cube, summing up the estimations of slices intersecting the cube. The result of the algorithm is the cube that corresponds to a fragment of the 3D image with the highest image quality assessment. The proposed approach allows organizing parallel processing of the slices to select the regions located inside the sample and to assess the image quality in this area. Image handling in the slice-wise mode is one from approaches to reduce the processing time of a tomographic image [5].

The method of selecting the region related to the sample assumes that there are areas of varying intensity or filled with different textures in the image of the sample, between which there are visible edges. We propose to apply the thresholding of the outcome of the variance filter [6] to detect the edges between regions. At the same time, if on the image of the slice there are only the edges of the holder, then they should be ignored. From the obtained convex regions for the stack of slices, we can easily determine whether the cube of a given size can be inscribed in them. Moreover, we can find the maximum possible size of the inscribed cube using an algorithm that determines the maximum rectangle that fits inside the connected region [7].

Over the past decade, several no-reference (blind) image quality metrics have been proposed [8-11]. Algorithms for calculating these quality metrics were trained and tuned on a set of natural 2D photos. They can assess the quality of 2D grayscale images with a bit depth of 8 bits per pixel. It was assumed that among the existing non-reference quality metrics we can find applicable for characterizing the quality of the slices of micro-CT images.

To use mentioned no-reference image quality metrics, we should convert images from 16 bits per voxel to 8 bits per voxel. Generally, intensities of images having 16 bits per voxel do not occupy the entire dynamic range. Thus, we need to increase the contrast in converting the images to 8 bits per voxel. Sometimes, it is advisable to increase the contrast in case of images with 8 bits per voxel too. The intensities of all 3D image slices should be normalized in the same range. The parameters for normalization are determined by means of analyzing the intensity histogram H of the central part of the 3D image. To calculate the histogram H, we perform a preliminary pass through the central part of the image, for which we indent 25% from each side of the image.

The lower bound l for intensities normalization is calculated using the statement [12]:

$$l = \min\left(\min\left\{i \middle| H[i] \geq H_0\right\}, \min\left\{i \middle| \sum_{k=0}^{i} H[k] \geq C_0\right\}\right), \tag{1}$$

where H_0 is the threshold for the height of the histogram column for dark tones; C_0 is the threshold for the area of the histogram in dark tones, functionally C_0 is equivalent to the percentile of H.

The upper limit u for intensities normalization is calculated with the formula:

$$u = \max\left(\max\left\{i \middle| H[i] \geq H_1\right\}, \max\left\{i \middle| \sum_{k=i}^{2^n-1} H[k] \geq C_1\right\}\right), \tag{2}$$

where H_1 is the threshold for the height of the histogram column for bright colors; C_1 is the threshold for the area of the histogram in bright colors; n is the bit depth, 8 or 16.

Normalization of the intensities of each slice I in the range [0, 255] is performed according to the formula:

$$I(r,c) = \begin{cases} 0 : I(r,c) \leq l, \\ \dfrac{255\left(I(r,c) - l\right)}{(u-l)} : l < I(r,c) < u, \\ 255 : u \leq I(r,c) \end{cases} \tag{3}$$

where (r, c) is the slice pixel coordinates, $r = 0 \ldots N - 1$, $c = 0 \ldots M - 1$; N is the number of rows in the image; M is the number of columns.

2.2. Region of sample selection in 2D slice

The algorithm for selecting the region belonging to the sample searches for a convex region, within which there are distinguishable edges between regions of different intensity. It is important to find the area inside the sample, but it is not necessary to accurately detect the boundary of the sample. Often,

the noise level in micro-CT images is quite high. Therefore, many well-known edge-detection filters are not applicable, as they react to noise. In addition, we are not interested in the edges themselves, but areas where there are changes in intensity. The variance filter allows getting an image in which relatively large values are in the pixels, around which there is a change in the intensity and relatively small values in uniform areas.

The variance filter is defined as [6]:

$$I_{\text{var}}(r,c)=\frac{1}{W^2}\sum_{i=0}^{W-1}\sum_{j=0}^{W-1}\left(I\left(r+i-\left[\frac{W}{2}\right],c+j-\left[\frac{W}{2}\right]\right)-\overline{I_W}(r,c)\right)^2, \quad (4)$$

where [ ] is the operator of taking the integer part; $I(r, c)$ is the intensity of a pixel with coordinates (r, c), $r = [W / 2] \ldots N - [W / 2] - 1$, $c = [W / 2] \ldots M - [W / 2] - 1$; the mean value $\overline{I_W}$ within the window is calculated as:

$$\overline{I_W}(r,c)=\frac{1}{W^2}\sum_{i=0}^{W-1}\sum_{j=0}^{W-1}I\left(r+i-\left[\frac{W}{2}\right],c+j-\left[\frac{W}{2}\right]\right). \quad (5)$$

The window size depends on the slice size, and it is selected about 100 by 100 pixels. Figure 2b shows the result of the variance filter for the slice in figure 1a. Thresholding of the outcome of the variance filter allows obtaining a binary image, in which the pixels are set to value 1 when the intensity varies in the local vicinity. Figure 2b shows the result of the thresholding. It should be noted that after the thresholding, several connected regions may form. To merge them into a single connected region, we use the morphological closing operation [13]. Several small areas can be located near the boundaries of the image. For instance, they can occur on the outer border of the holder. To exclude these undesirable regions from consideration we process only the connected region with the largest area. For this region, we calculate the convex hull and fill it with values 1. The resulting region protrudes approximately half to two-thirds of the size of the variance filter window from the sample region. To ensure that the region is inside the sample region, a morphological erosion filter [13] is applied with the size of the structural element equal to the size of the variance filter window.

Note that the image of the slice may be missing a fragment relating to the sample. The proposed algorithm allows detecting such a situation. We make a conclusion about this situation based on the area and shape of the largest detected region after the application of the closing operation. Also, according to the results of the sample area selection on the slice, the algorithm produces recommendations for the operator of the micro-CT system. For example, if the sample is significantly displaced from the center of the slice, then it is probably possible to reconstruct an image of better quality if you re-shoot the shadow projections by placing the sample in the center.

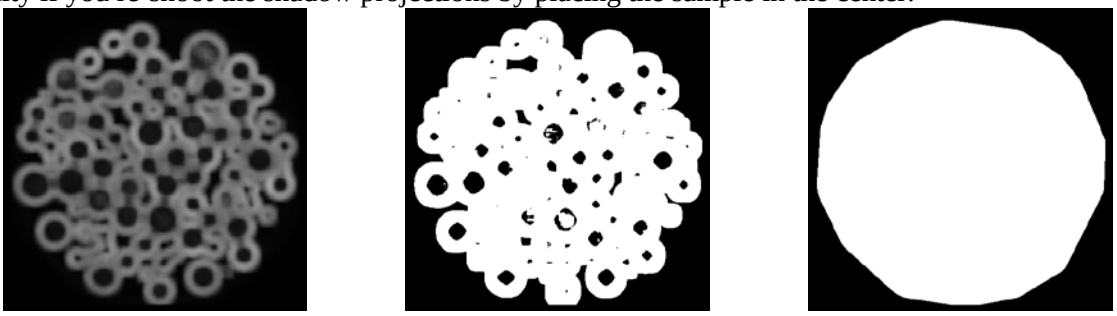

a) b) c)

Figure 2. Illustration of the sample region selection stages for the slice from figure 1a: (a) the result of the variance filter; (b) the result of the thresholding of image from figure 2a; (c) a convex region constructed along the outer boundary of region from figure 2b.

2.3. Analysis of the use of no-reference quality metrics for micro-CT images

At present, a sufficiently big number of no-reference image quality metrics has been proposed. Such metrics make possible to evaluate the quality based on the image only without the reference. Part of the metrics is designed to assess one factor affecting the quality, for example, the blurriness level [14].

Others claim to universality. We evaluated the following algorithms for assessing of quality of slices of micro-CT image: BIQI (Blind Image Quality Index) [8], BRISQUE (Blind Referenceless Image Spatial Quality Evaluator) [9], NIQE (Natural Image Quality Evaluator) [10] and OG-IQA (Oriented Gradients Image Quality Assessment) [11].

The considered algorithms were trained on natural photos, for instance, from the LIVE data set [15]. This data set, in addition to undistorted photos, contains images that have been distorted. Several types of distortion were used: additive white Gaussian noise, Gaussian blur, JPEG and JPEG2000 compression artifacts. However, this dataset is rather idealistic, because only one type of distortion affects an image at the same time. After interviewing many observers, an estimate of quality for each image from the set was calculated based on the pairwise comparison.

The BIQI algorithm [8] implements a two-step approach to assess the quality of the images. This approach is based on a natural scene statistic (NSS) and the assumptions that natural images have certain statistical properties, and distortions change these statistical characteristics in such a way that the type and degree of distortion can be estimated with a high confidence level. The first step in BIQI is an identification of distortion type. The second stage is an estimation of the strength of the distortion. Features for learning are taken from the model of natural scenes in the wavelet domain [16]. The models for classification and regression are trained by support vector machine (SVM) on data from the LIVE dataset. The BRISQUE method [9] uses the features of the NSS model calculated in the spatial domain [17]. A single regression model for all distortion types is trained on images from LIVE dataset using SVM method. The NIQE [10] technique constructs of a multivariate Gaussian distribution (MVG) of statistical features based on the statistical model of natural scenes in the spatial domain [17]. The quality of the estimated image is defined as the distance between the multidimensional normal distribution of this image characteristics and the reference MVG obtained as a result of training on the features of pristine undistorted images. The OG-IQA [11] algorithm analyzes the correlation structure of the gradient orientation in the image. The idea is that the orientation of the local gradients contains significant information about the naturalness of the image, and when distortions appear, this information changes in a certain way. The AdaBoost algorithm is used to train the regression model.

Initially, we assumed that these metrics can be used for an absolute quality assessment of micro-CT images, i.e. regardless of the equipment used and the sample analyzed. However, from the experiments, we saw that the metrics are not applicable for assessing the quality of images for samples of different rocks, because frequently the results did not correspond to the expert's opinion and the physical parameters of the experiments. However, for a comparative quality assessment of slices from one sample, the results were quite reasonable.

To study the applicability of these criteria for the comparative quality assessment of the slices from one sample, we formed a set of 10 images obtained as follows. We obtained six images by scanning the same sample with different exposure times. The noise level is directly dependent on the exposure time. The highest noise level corresponds to the shortest exposure. For two of these six images, we additionally reconstructed two images with a binning and a reduced number of projections. Binning is the process of combining the charges of neighboring pixels on an image sensor into one "superpixel". In tomographic reconstruction, binning is lowering the spatial resolution due to summation the values of neighboring pixels, which leads to an increase in the signal-to-noise ratio. Using fewer projections for reconstruction causes noise-like artifacts.

For these 10 images, it is known how they are ranked according to their quality. For the central part of these images, we calculated the quality assessment by several quality metrics. Table 1 contains the number of errors in image rankings using considering no-reference quality metrics. The number of errors is counted as the number of images that must be removed from the series to obtain a properly sorted sequence by quality. The best result was shown by NIQE metrics, which made two mistakes with images reconstructed with binning.

NIQE advantage was expected. This metrics is less associated with a fixed set of distortions of the LIVE dataset and uses a simpler model which is less tended to overfit. Moreover, for NIQE we built own MVG model of high-quality micro-CT images instead of photos from LIVE dataset. Further adjustment of this model may lead to improved results.

Table 1. The number of errors in the quality ranking of micro-CT images using non-reference quality metrics.

Quality metrics	Errors count
BIQI	4
BRISQUE	4
OG-IQA	6
NIQE	2

2.4. Algorithmic optimization

We achieve a high speed of handling of images due to parallel processing and the use of optimized algorithms. An example of algorithmic optimization is the implementation of a variance filter via integral images. In the integral image *IntI*, each pixel with coordinates (*r*, *c*) is equal to the sum of the pixels of the image *I* located to the left and above (*r*, *c*) [18]:

$$IntI(r,c)=\sum_{\substack{r'\le r\\ c'\le c}} I(r',c'). \tag{6}$$

IntI can be calculated in a single pass through the image *I* by the following statement:

$$IntI(r,c)=I(r,c)+I(r,c-1)+I(r-1,c)-I(r-1,c-1). \tag{7}$$

The sum of the pixels in the square window for the image *I* via the integral image *IntI* is calculated as:

$$\begin{aligned} S(r,c)=&IntI\left(r+\left[\frac{W-1}{2}\right],c+\left[\frac{W-1}{2}\right]\right)+IntI\left(r-\left[\frac{W}{2}\right],c-\left[\frac{W}{2}\right]\right)\\ &-IntI\left(r-\left[\frac{W}{2}\right],c+\left[\frac{W-1}{2}\right]\right)-IntI\left(r+\left[\frac{W-1}{2}\right],c-\left[\frac{W}{2}\right]\right), \end{aligned} \tag{8}$$

where *W* is the window size; the coordinate (*r*, *c*) is in the center of the window.

With the help of integral images, we can quickly perform the operations of the summation and averaging of rectangular image blocks. The area of integral images application is expanded by calculating such images for squares and higher powers of pixel values [19]. If we additionally calculate the integral image of *IntI2* for I^2 (via the formula (7)) and the sum of pixels in the square window S_2 (using formula (8)), then the variance filter can be calculated as:

$$I_{\text{var}}(r,c)=\frac{1}{W^2}\left(S_2(r,c)-\frac{S(r,c)^2}{W^2}\right). \tag{9}$$

Table 2 contains the processing time of a slice of 4000×4000 pixels by three various implementations of variance filter. We estimated the time for a single-threaded C++ program on a laptop with CPU Intel Core i7 2.6 GHz. The slowest approach is the implementation of the filter directly via formulas (4) and (5) in several nested loops. It is much faster to calculate the variance from the histogram, which during the window movement across the image is not recalculated completely but is updated. Finally, the fastest way is to calculate the local variances via integral images. The integral images *IntI* and *IntI2* require a larger amount of memory in comparison with *I*, but in our task, this is not a limitation.

Table 2. The variance filter processing time for a slice of 4000×4000 pixels.

Method	Processing time, s
In several nested loops	4.3
Via histogram	1.1
Via integral images	0.5

3. Results and conclusions

We tested about one hundred 3D micro-CT images that had from 1000 to 2000 slices. The region inside the sample was selected correctly for all cases. The results of the automatic selection of regions for the slices from figure **1** are shown in figure 3.

To test the algorithm for cropping of 3D fragment having the highest visual quality, we developed a software tool for generating a synthetic image of the micro-CT slice (see figure 4). This tool allows adjusting the sample size, the level of additive or multiplicative Gaussian white noise, the contrast, the radius of blurring filter, and the intensity of the holder region. From these synthetic slices, we formed a 3D image in which the noise level increased from the central slice to the top and bottom. For the slices of this 3D image, we calculated inverted and normalized NIQE quality metrics Q. As expected, the quality assessment Q is correlated with the noise level and is decreased from the central slice to top and bottom. Our algorithm identifies the central region as having the highest quality because the sum of quality assessments for the central slices is maximum (see figure 5). Background of the graph is a cross-section of the generated 3D image.

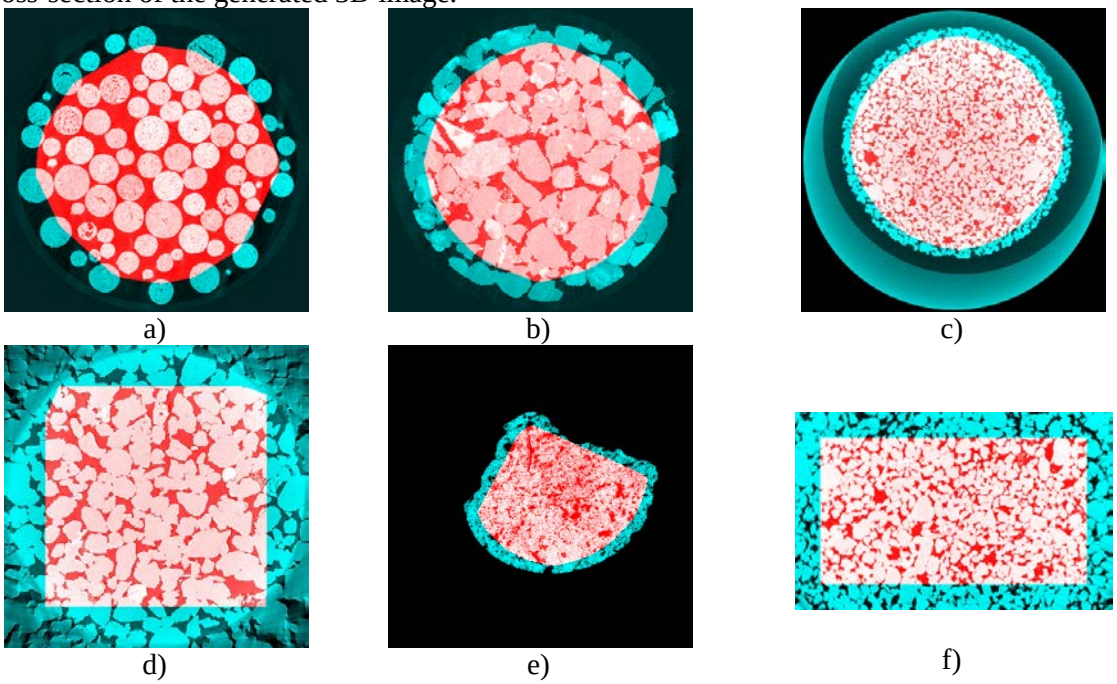

a) b) c)

d) e) f)

Figure 3. The results of the algorithm for the selection of areas related to the sample for images from figure 1.

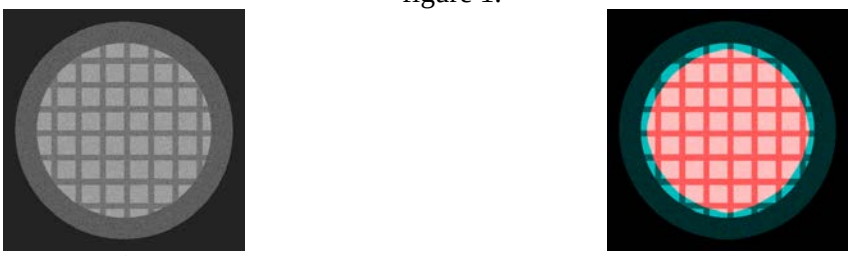

a) b)

Figure 4. Synthetic image of the slice (a) and the result of the area related to the sample selection (b).

Outcomes for real micro-CT images of rocks and granular materials are in good agreement with expert opinion, except regions damaged by X-ray tomography-specific local defects, for example, ring artifacts and intensity distortions due to high-dense inclusions. The existing no-reference image quality metrics can give a relative estimation of the noise level and sharpness for the slices from a single image, but do not consider tomography-specific artifacts. Figure 6 demonstrates a plot with a cross-section of normalized NIQE quality metrics for slices of real micro-CT image.

The processing time of a 4000×4000×2000 voxel 3D image takes less than 6 minutes on a laptop with CPU Intel Core i7 2.6 GHz, 8 Gb RAM, SSD. The use of the proposed algorithm allows reducing the operator's spent time on the selection of a 3D micro-CT image fragment for further modelling and to excludes subjective judgments from this stage.

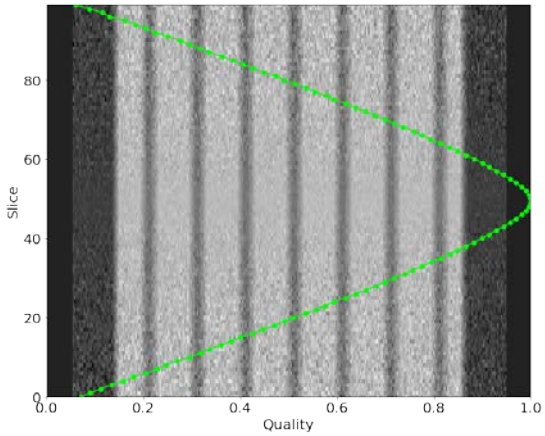

Figure 5. The graph of normalized NIQE quality estimation on the synthetic 3D image slices, where the noise level increases from central slice to top and bottom.

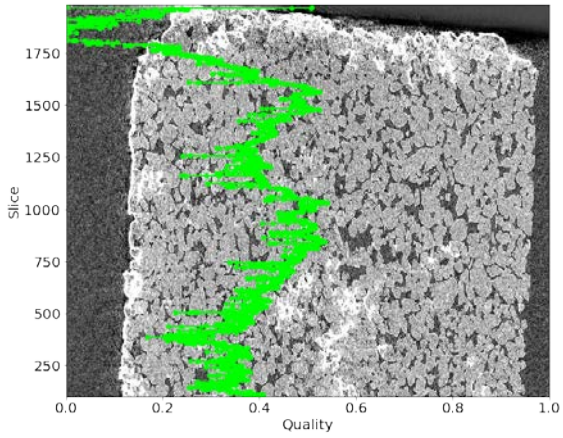

Figure 6. The graph of normalized NIQE metrics for slices of the real 3D image.

4. References

[1] Safonov I, Yakimchuk I and Abashkin V 2018 Algorithms for 3D particles characterization using X-ray microtomography in proppant crush test *J. of Imaging* **4** 134

[2] Koroteev D A, Dinariev O, Evseev N, Klemin D V, Safonov S, Gurpinar O M, Berg S, van Kruijsdijk C, Myers M, Hathon L A, de Jong H and Armstrong R 2013 Application of digital rock technology for chemical EOR screening *Proc. of the SPE Enhanced Oil Recovery Conf.* 165258

[3] Dinariev O and Evseev N 2016 Multiphase flow modeling with density functional method *Computational Geosciences* **20** 835-856

[4] Buzug T M 2008 *Computed Tomography: From Photon Statistics to Modern Cone-Beam CT* (New York: Springer Science & Business Media)

[5] Smelkina N A, Kolsanov A V, Chaplygin S S, Zelter P M and Khramov A G 2017 Pulmonary emphysema recognition by CT scan *Computer Optics* **41(5)** 726-731 DOI: 10.18287/2412-6179-2017-41-5-726-731

[6] Fabijańska A 2011 Variance filter for edge detection and edge-based image segmentation *MEMSTECH*

[7] van Droogenbroeck M and Piérard S 2011 Object descriptors based on a list of rectangles: method and algorithm *Int. Symp. on Mathematical Morphology and Its Applications to Signal and Image Processing*

[8] Moorthy A K and Bovik A C 2010 A two-step framework for constructing blind image quality indices *IEEE Signal processing letters* **17** 513-516

[9] Mittal A, Moorthy A K and Bovik A C 2012 No-reference image quality assessment in the spatial domain *IEEE Transactions on Image Processing* **21** 4695-4708

[10] Mittal A, Soundararajan R and Bovik A C 2013 Making a “completely blind” image quality analyzer *IEEE Signal Processing Letters* **20** 209-212
[11] Liu L, Hua Y, Zhao Q, Huang H and Bovik A C 2016 Blind image quality assessment by relative gradient statistics and adaboosting neural network *Signal Processing: Image Communication* **40** 1-15
[12] Safonov I V, Kurilin I V, Rychagov M N and Tolstaya E V 2018 *Adaptive Image Processing Algorithms for Printing* (Singapore: Springer)
[13] Soille P 2004 *Morphological Image Analysis: Principles and Applications* (New York: Springer Science & Business Media)
[14] Asatryan D G 2017 Image blur estimation using gradient field analysis *Computer Optics* **41(6)** 957-962 DOI: 10.18287/2412-6179-2017-41-6-957-962
[15] Sheikh H R, Sabir M F and Bovik A C 2006 A statistical evaluation of recent full reference image quality assessment algorithms *IEEE Transactions on Image Processing* **15** 3440-3451
[16] Srivastava A, Lee A B, Simoncelli E P and Zhu S C 2003 On advances in statistical modeling of natural images *J. of mathematical imaging and vision* **18** 17-33
[17] Ruderman D L and Bialek W 1994 Statistics of natural images: Scaling in the woods *Advances in neural information processing systems*
[18] Crow F C 1984 Summed-area tables for texture mapping *ACM SIGGRAPH computer graphics* **18** 207-212
[19] Phan T, Sohoni S, Chandler D M and Larson E C 2012 Performance-analysis-based acceleration of image quality assessment *SSIAI* 81-84